WAVEFORMS IN THE ARTERIAL TREE

A. G. Lindgren, K. Kerr, L. Antonelli, and Y. Sun

Department of Electrical Engineering
The University of Rhode Island
Kingston RI 02881

ABSTRACT

System identification techniques were employed to characterize the dynamics in the arterial system. Arterial pressure and flow waveforms were obtained from computer simulations using a complex model and from experiments in domestic swine. Transfer functions were identified by using an iterative least-squares approach. It was shown that the aortic input impedance can be sufficiently characterized by a 1st-order system and the transfer function between aorta and femoral artery is dominated by a 2nd-order system. Within a scale factor the estimated aortic flow waveform matched well with the measured (less than 1% error). Thus, the proposed method provides for the cycle-by-cycle determination of flow waveform from aortic root pressure and should be useful for studying circulatory dynamics and regulatory control mechanisms.

1. INTRODUCTION

Various models have been proposed and developed to simulate the dynamic behavior of waveforms in the arterial tree. They are phenomenological models in that they effectively reproduce waveforms typical of that experienced in the cardiovascular system under various disease conditions. A functional block diagram of one specific model is shown in Fig. 1. The detail composition of both the arterial tree and heart dynamic models contain (in terms of the electrical analogs) linear, time-varying and nonlinear resistors, capacitors and inductors, see references [1-2]. The action of the aortic valve, under conditions representative of most arterial behavior, is sufficiently modeled by a diode. During diastole, where the aortic valve is closed or the diode acts like an open switch, the aortic flow is zero. Using system identification techniques on the arterial root pressure (ARP) waveform, it is possible to find a model of the arterial tree dynamics during diastole that permits the form of the arterial flow (AF) waveform to be determined during systole. Since AF is difficult to measure, the determination of AF from ARP is a useful tool in the study of cardiac function. The same assumptions of linearity (of the arterial tree) are then applied to analysis of actual arterial pressure waveforms in domestic swine. Experiments to determine AF and stroke volume from pressure waveforms in domestic swine show the usefulness of the technique. The interaction of stroke volume and heart rate with respiration is also displayed. Since the pressure waveforms are measured in several locations in the swine experiments,

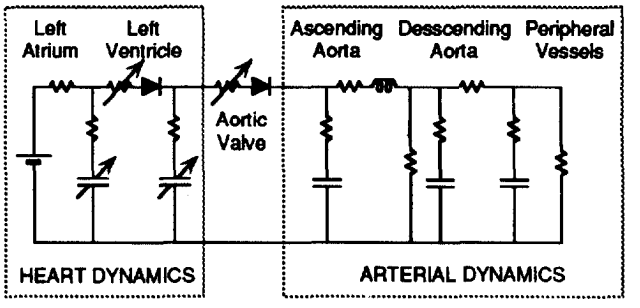

Figure 1: Simulation model of heart and arterial tree.

the dynamic transfer function from one location to another can also be determined by system identification techniques. Models from these transfer functions are then developed for the arterial tree. This paper describes these techniques and presents the results derived from the processing of pressure waveforms in the arterial tree.

2. THE DATA

In-vivo data was obtained from experiments on domestic swine originally designed to evaluate intraaortic balloon pump performance. Pressure was measured at three different sites by 1) a micromanometer-tip catheter in the aortic root, 2) an intraaortic balloon catheter with a fluid-filled lumen open to the distal end of the balloon in the descending aorta, and 3) a fluid-filled catheter in the femoral artery, see Fig. 2. The measured waveforms are shown in Fig. 3. The subject was on a respirator and the effect of the insertion of air on the ECG is visible in Fig. 4a. Also shown in Fig. 4b is the modulation of ARP by respiration (note the change in time scale from Fig. 3); similar effects on the descending aortic pressure (DAP) and the femoral arterial pressure (FP) were observed.

3. SYSTEM IDENTIFICATION

There are many approaches to develop algorithms for system identification, see [3,4], and various algorithms are readily available (e.g. Matlab System Identification Toolbox). Since the techniques described in this paper include some variations of the standard approach, a brief derivation is presented for completeness. The notation used is a

1058-6393/95 $4.00 © 1995 IEEE

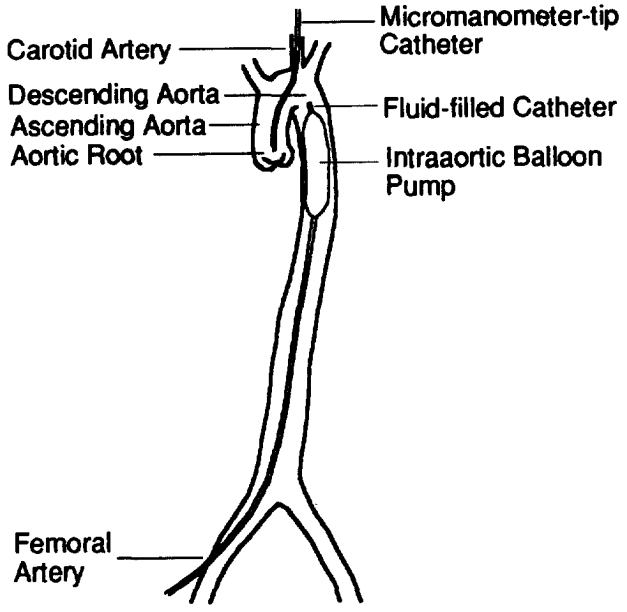

Figure 2: Positioning of catheters in swine aorta.

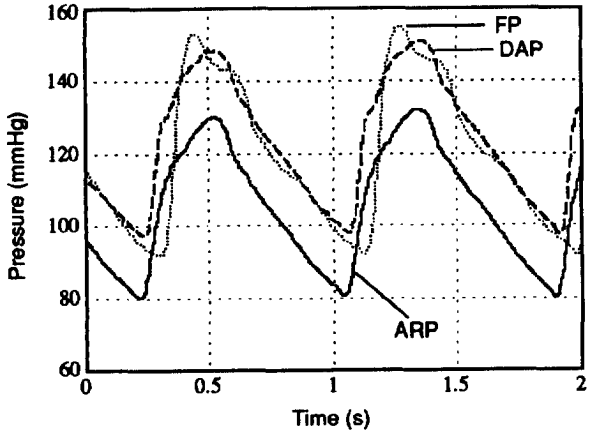

Figure 3: Aortic root pressure (ARP), descending aortic pressure (DAP), and femoral arterial pressure (FP) from swine.

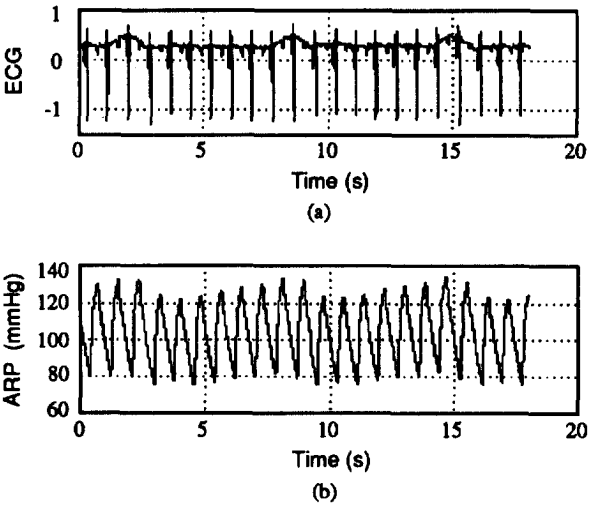

Figure 4: (a) ECG; (b) ARP from swine.

mixture of the standard mathematical forms and MATLAB format that should be self explanatory.

Given an unknown transfer function $h(z) = b(z)/a(z)$ we seek to match its output by adjusting the parameters $\hat{a} = [1; \hat{\alpha}]$ and $\hat{b}$ of the model $\hat{h} = \hat{b}(z)/\hat{a}(z)$ (all estimated quantities are labelled with "^"), see Fig. 5a. In the time domain, when the input is an impulse, the k-by-1 output error is $e = [h - \hat{h}] = h - X\hat{b}$, where X is the k-by-n matrix corresponding to the time sequence of the n signals (system state) generated by the recursive part of the model filter. The objective is to minimize the performance criterion

$$J = \|h - \hat{h}\|^2 = \|h - X\hat{b}\|^2. \quad (1)$$

To simplify the derivation we consider the case where $h(0) = 0$, i.e., h =[h(1), h(2), ..., h(k)] and $\hat{h}$ is a linear combination of the model state X. Given the (n+1) vector $\hat{a}$ and a k vector p = [flipud($\hat{a}$); zeros(k-n+1)], we then form the (k by n) matrix A whose first column is p and each successive column is rotated down one element. With this definition A has the property

$$A^T X = 0 \ \text{(the null matrix)} \quad (2)$$

and the projection matrices $AA^\dagger$ and $XX^\dagger$ are orthogonal and complementary. The $\dagger$ sign indicates the generalized inverse. Minimizing (1) wrt the coefficient vector $\hat{b}$ yields

$$J_{\hat{a}} = \|(I - XX^\dagger)h\|^2 = \|AA^\dagger h\|^2 = h^T A(A^T A)^{-1} A^T h. \quad (3)$$

Since it can be shown that $A^T h = H\hat{a}$, where the (k-n)-by-(n+1) matrix is given by

$$H = \begin{bmatrix} h(n+1) & h(n) & \dots & h(1) \\ h(n+2) & h(n+1) & \dots & h(2) \\ \dots & \dots & \dots & \dots \\ h(k) & h(k-1) & \dots & h(k-n) \end{bmatrix}, \quad (4)$$

and if we define $R = A^T A/(\hat{a}^T\hat{a})$, then (3) can be written as

$$J_{\hat{a}} = \hat{a}^T H^T R^{-1} H\hat{a}/(\hat{a}^T\hat{a}). \quad (5)$$

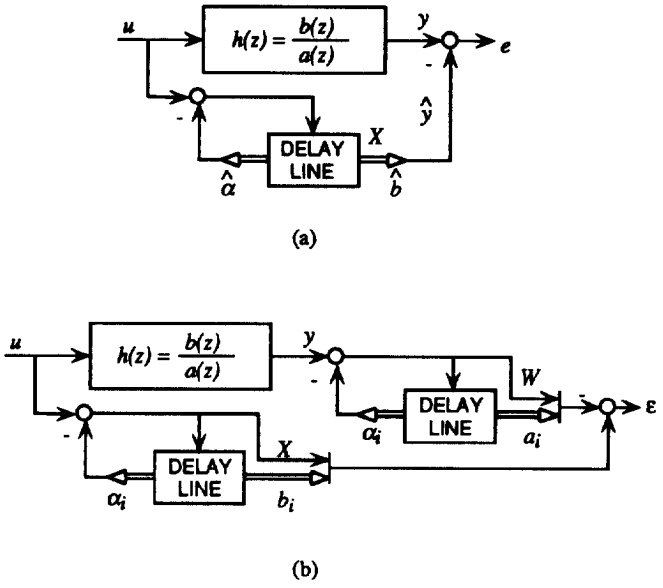

Figure 5: (a) Output error model, note $\hat{a} = [1; \hat{\alpha}]$; (b) system identification model, $a_i = [1; \alpha_i]$.

Minimization of (5) is an eigenvalue problem where the solution is the eigenvector corresponding to the smallest eigenvalue. Since $R = R(\hat{a})$ is a function of $\hat{a}$ we need to iterate this result. $R = I$ can be used to initiate the process. Also note that a smaller row dimension H can be used, in particular one that starts further along on the impulse response, i.e., H(1,n+1) = h(m), where m > 1.

When the input is other than an impulse, the following algorithm was used to compute $\hat{a}$ and $\hat{b}$. If we have an estimate of $\hat{h}(z) = b_i(z)/a_i(z)$ the output error is (see Fig. 5b)

$$\begin{aligned} e(z) &= y(z) - y\hat{h}(z) = [b_i(z)/a_i(z) - b(z)/a(z)]u(z) \\ &= [u(z)/a_i(z)]\delta b_i(z) - [y(z)/a_i(z)]\delta a_i(z) \\ &= x(z)\delta b_i(z) - w(z)\delta a_i(z) \end{aligned} \quad (6)$$

where $\delta a_i = a - a_i$ and $\delta b_i = b - b_i$ is the correction in the (coefficients of the) polynomials. If $y(z) - \hat{y}(z)$ is now subtracted from each side of (6) and we define $a_{i+1} = a_i + \delta a_i$ and $b_{i+1} = b_i + \delta b_i$, then we obtain

$$x(z)b_{i+1} - w(z)a_{i+1} = \epsilon(z) \quad (7)$$

where $\epsilon(z)$ accounts for extraneous errors. In the time domain the k-by-(n+1) matrix ε can be written as

$$Xb_{i+1} - Wa_{i+1} = \varepsilon \quad (8)$$

where X and W are k-by-(n+1) matrices and b_{i+1} and a_{i+1} are (n+1)-by-1 matrices. The performance is defined by

$$J = \|\varepsilon\|^2 = \|Xb_{i+1} - Wa_{i+1}\|^2 \quad (9)$$

and optimizing wrt b_{i+1} yields

$$\begin{aligned} J_a &= \|(I - XX^\dagger)Wa_{i+1}\|^2 = a_{i+1}^T W^T (I - XX^\dagger)Wa_{i+1} \\ &= a_{i+1}^T [R_{ww} - R_{wx}R_{xx}^{-1}R_{wx}^T]a_{i+1} \end{aligned} \quad (10)$$

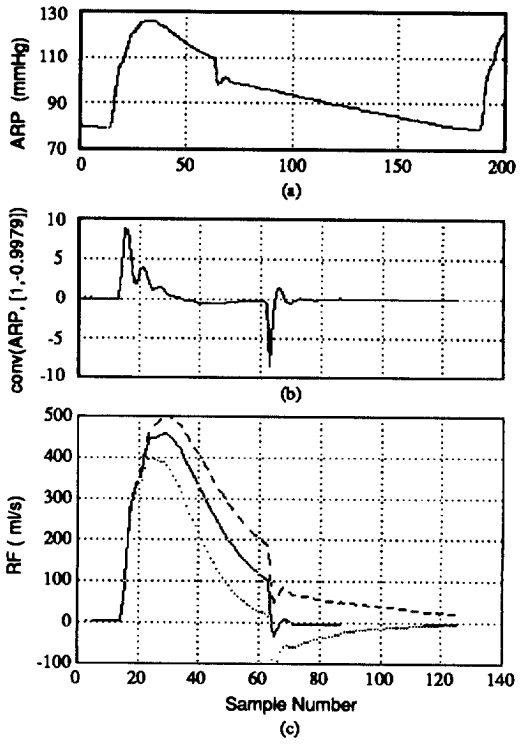

Figure 6: (a) Simulated ARP waveform; (b) convolution of ARP with [1,-0.9979]; (c) reconstructed flow (RF) by deconvolution of waveform in (b) with [1,-0.971] (solid), [1,-0.98] (dotted) and [1,-0.95] (dashed), respectively.

where $R_{ww} = W^T W$, $R_{wx} = W^T X$ and $R_{xx} = X^T X$. The goal is to find a_{i+1} that minimizes J_a. This is again an eigenvalue problem similar to (5). Since X and W depend on a_i, we use a_i in X and W to solve for a_{i+1}, then update X and W with a_{i+1} and compute a_{i+2}. This iteration continues until the process converges. Convergence is normally very rapid. With $\hat{a}$ (= lim a_i; $i \to \infty$) known, the computation of $\hat{b} = X^\dagger h$ is direct. The initial computations begin with $X = U$ and $W = Y$ (or a_0 = [1; zeros(n,1)]). If there is an error in modeling $h(z) = b(z)/a(z) + \varepsilon_0(z)$, then as a_i converges to "a" the error ε approximates to ε_0.

4. TECHNIQUE FOR FLOW DETERMINATION FROM ARP

ARP and AF from the simulation of Fig. 1 are shown in Fig. 6a&b (solid curve). The portion of the ARP waveform after the dicrotic notch, where AF is zero (diastole), contains information about the dynamics or impedance of the aortic tree. It is the response to the volume injected by the AF waveform during systole and is like an equivalent impulse response. Essentially, the flow waveform determines the state of the dynamic system established at the end of systole. In diastole the state decays producing the diastolic portion of the ARP waveform. By treating the ARP during diastole as an impulse response, equation (5) can be used

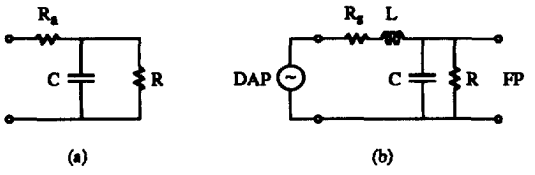

Figure 7: (a) Windkessel model of aortic input impedance; (b) electrical analog of transfer function from DAP to FP.

to find the coefficients of the characteristic equation (or the poles of the "impedance" transfer function) of the arterial dynamics. It now remains to determine the zeros of the arterial dynamics.

For the ARP waveform in Fig. 6a, the section between samples 80 and 170 was used to form the H matrix in (4). By viewing the singular values of $F = H^T R^{-1} H$ the system is found to be dominated by first order dynamics with characteristic equation $a(z) = z - 0.9979$. Because the system is first order determination of the zeros (or numerator coefficients) is readily accomplished. Figure 6b shows the result of convolving the ARP waveform with the denominator coefficients [1,-0.9979]. Since we know the AF waveform is zero during diastole, we can deconvolve the waveform in Fig. 6b with trial numerator coefficients (or zero locations). The result is shown in Fig. 6c for several zero locations (0.95, 0.971, and 0.98). The desired response is obtained for a zero located at $z = 0.971$. To achieve the flow which is depicted in Fig. 6c, the reconstructed flow (RF) waveform was amplitude scaled to minimize the difference the two waveforms (K = scale factor = AF^T RF / AF^T AF). For this example $K = 11.5$ and the error waveform EF = AF - K RF is -40 dB below AF. That is, the normalized mean square error $J = EF^T$ EF / AF^T AF $= 5 \times 10^{-5}$. RF and AF are essentially overlapped in Fig. 6c. Similar analysis performed on a wide variety of waveforms corresponding to different cardiac conditions gave similar results. Accuracy of less than 1% was achieved in all cases and the above accuracy represents the typical result. This accuracy, we believe, is generally beyond that required in most research on circulation dynamics.

Thus, within a scale constant, we can reconstruct the aortic flow (AF) waveform from the aortic root pressure (ARP) waveform for data obtained from the simulations described in [1]. Practical methods to determine the scale factor or absolute value of flow are at best illusive. The results for the complicated simulation depicted in Fig. 1 produced a modeling of the aortic impedance as shown in Fig. 7a. This is the Windkessel model [5] for aortic dynamics and, if this result holds for actual data, essentially validates the use of such simple low-order dynamics for studies of the aortic tree. For this simulated data the values in the Windkessel model are RC = 2.38 and R/R_a = 13.0. The values of this model were derived from the s-plane locations of the poles (and zeros), s = ln(z)/t_s, where t_s is the sampling time and $t_s = 0.005 = 5$ ms.

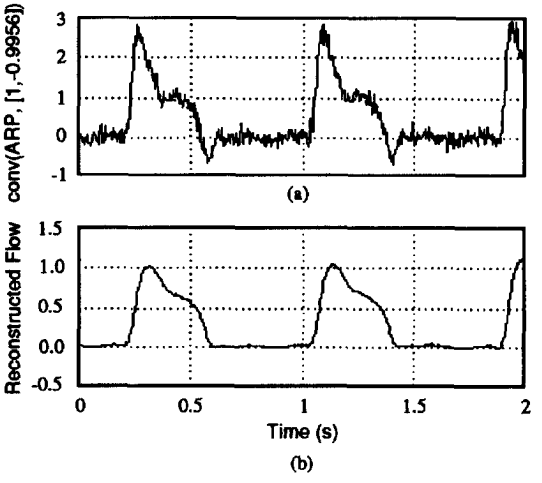

Figure 8: (a) Convolution of ARP in swine with [1,-0.9956]; (b) reconstructed flow in swine, deconvolution of waveform (a) with [1,-0.91].

5. FLOW RECONSTRUCTION FROM ARP IN SWINE

The technique of section 4 was applied to the ARP data from domestic swine. Similar to the situation using simulated data, the aortic impedance for the swine data was found to be predominantly first order. For the data examined the pole location was $z = 0.9956$ and convolving the denominator coefficients with the ARP yields the waveform in Fig. 8a. The result for a zero located at $z = 0.91$ is also shown in Fig. 8b and within a scale factor, we believe this is nearly the AF waveform. The sensitivity of the result to zero locations for values around $z = 0.91$ was low. We believe this is accounted for by the relatively small value of the zero location and it means the resistor R_a is small or negligible. This will also be supported by later results. For this swine data the values in the Windkessel model are RC = 1.134, R/R_a = 20.4 or R_a/R = 0.049 and T/RC = heart-period/time-constant $\cong$ 0.75.

Measurements of actual flow (AF) were only available to us in strip chart recordings. For these measurements ARP and AF waveforms were generated to match the recordings and are shown in Fig. 9. Flow was then computed from the pressure waveform and is shown (dashed) in Fig. 9a. An ARP was also reconstructed from the swine AF waveforms and is shown (dashed) in Fig. 9b. For this example RC = 1.67 and R/R_a = 19.6.

6. IDENTIFICATION OF TRANSFER FUNCTION BETWEEN AORTIC ROOT AND FEMORAL ARTERY IN SWINE

Identification of the transfer function between the aortic root and other locations in the aortic tree is accomplished by use of (10). Here the ARP waveform is the input (u) and

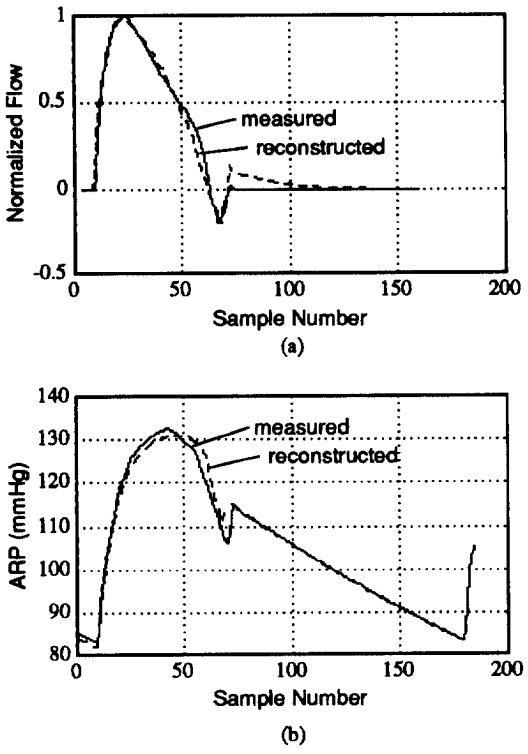

Figure 9: (a) Measured (solid) and reconstructed (dashed) ARP; (b) measured (solid) and reconstructed (dashed) AF.

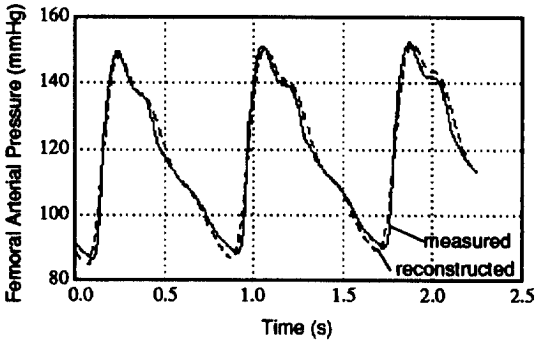

Figure 10: Femoral pressure (solid) and reconstructed femoral pressure from ARP (dashed).

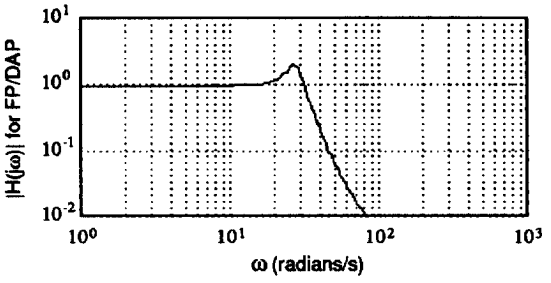

Figure 11: Frequency response of the transfer function between descending aorta and femoral artery.

the femoral pressure waveform is the output (y) as described in section 2. Forming the initial X matrix we use the ARP and the initial W is constructed from FP waveform. It is found that the dynamics are approximated by a second-order system. Iterating, as described in section 2, yields $a(z) = z^2 - 1.9304z + 0.9441$ and $b(z) = -0.0219z + 0.0376$. The poles are at $z = 0.9652 + j0.1117$ and a zero at $z = 1.715$. The match between the femoral pressure waveform is shown in Fig. 10. Again the response is closely matched by a low-order (second order) system. The non-minimal phase nature of the sytem (zero location outside the unit circle in the z-plane) we believe is due to the system attempting to match a transportation delay between the aortic root and the femoral artery. By delaying the input signal it was possible to locate the zero inside the unit circle and realize the representation of the arterial tree dynamics by a passive model.

Because the solid-state sensor was not calibrated with the fluid-filled transducer, see the apparent scale factor difference between ARP and DAP in Fig. 3, the transfer function possessed a gain greater than unity at the D.C. frequency. To address this problem, the transfer function between descending aorta and femoral artery was also determined. The DAP waveform is similar to the ARP waveform with a small delay. The frequency response between descending aorta and femoral artery is shown in Fig. 11 and is essentially identical with that from aortic root to femoral artery except for a scale factor in amplitude. The D.C. gain for this transfer function was 0.9724, or near unity. This is as expected and confirms that the series resistance in the aorta is small. This will be quantified shortly. It is noted that the apparent increase in the amplitude of the pressure waveform between descending aorta and femoral artery is not due to the presence of any active components in the aortic tree dynamic model. It is explained by the dynamic behavior of the passive components that make up our dynamic model, $H(z) = b(z)/a(z)$. Basically, the harmonics (particularly the fourth harmonic) in the waveform at aortic root are amplified and undergo phase shifts in their transmission through this passive system (model). The response of a model with no zero was also computed and found to match the FP waveform nearly as well as the "output error model" above. The D.C. gain for this circuit from DAP to FP was also 0.9724 and the electrical analog of this model of the aortic tree is that given in Fig. 7b. Note, as described above, the serics resistor is observed to be relatively small. The values of this model are $R_s/R = 0.0284$, $LC = 0.001821$, $RC = 0.1007$, $R_s/L = 1.569$ and $\omega_0 = \sqrt{1/LC} = 23.43$.

7. STROKE VOLUME AND RESPIRATION

Stroke volume is the total amount of fluid pumped from the heart into the aorta in one cycle. We calculate it by integrating the flow over one cycle. Figure 12 shows the integral of AF in Fig. 8b and is seen to be relatively constant following the flow pulses (during diastole). The time location of the R-wave of the ECG is also displayed in Fig. 12 and is seen to occur shortly before the next AF pulse. Stroke

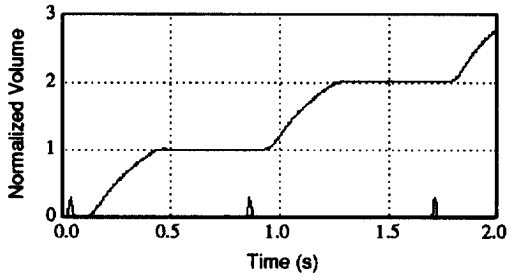

Figure 12: Normalized volume with R-wave location.

volume is calculated as the change in the volume level that results during the time between R-waves. Again, as with flow, volume is determined only within a scale factor of actual volume. Figure 13a shows the ECG of Fig. 4a along with the stroke volume as calculated above. The R-waves are numbered 1 through 22 and the value of the "normalized" volume pumped after the n^{th} R-wave is plotted at sample n in Fig. 13b (solid). Data for several experiments showed similar behavior. The period between the n^{th} and $(n+1)^{th}$ R-wave for this experiment is also plotted at sample n in Fig. 13b (dashed). Over a variety of similar experiments the period 'T' was found to be more random; in some instances the heart-rate was increasing or decreasing, and in other experiments, little change in the period was observed. Comparison of Fig. 13a&b. indicates a clear correlation (or interaction) of stroke volume with respiration.

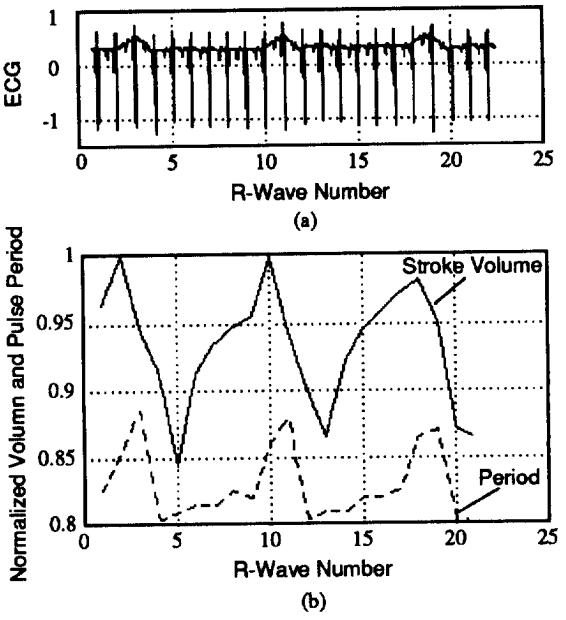

Figure 13: (a) ECG; (b) normalized stroke volume (solid) and cardiac period (dashed).

8. CONCLUSIONS

This paper has sought to demonstrate the potential of applying signal processing and system identification techniques to waveforms in the arterial tree. It has shown the validity of modeling the arterial dynamics with models of low-order. With such "simple" models, correlation of the model parameters with various circulation problems may permit the tracking of such parameters to monitor clinical therapies. A first step we are attempting is to take various phenomenological models, such as those in [1-2], and have them more closely match actual waveforms by appropriate settings of the model parameters. That is, to harden the parameters to more accurately reflect the processes they model. Evaluation of model parameters may aide diagnosis. In another study, use of arterial tree models is directed at the control of cardiac assist devices to maximize their effectiveness. The system identification method described in this study provides the cycle-by-cycle information of the change in stroke volume. This information should be useful for studying the effects of baroreflex and systemic autoregulatory control on hemodynamics [6] and the mechanisms of heart rate variability [7].

9. REFERENCES

[1] Y. Sun, "Modeling the dynamic interaction between left ventricle and intraaortic balloon pump," Am. J. Physiol. 261 (Heart Circ. Physiol. 24): H664-H672, 1988.

[2] J. S. Janicki, S. G. Shroff, and K. T. Weber, "Influence off Extracardiac forces on the cardiopulmonary unit" and K. B. Campbell, J. A. Ringo, N. S. Peterson, "Sensitivity analysis of interaction between the left ventricle and the systemic arteries," Chapters 12 & 13 in *Ventricular/Vascular Coupling*, Ed. by F. C. P. Yin, New York: Springer-verlag, 1987.

[3] L. Ljung, *System Identification Theory for the User.* Englewood Cliffs, NJ: Prentice-Hall, 1987.

[4] A. Kaelin, A. G. Lindgren, and G. S. Moschytz, "Simplified adaptive IIR filters," IEEE Trans. CAS, in press.

[5] D. A. McDonald, *Blood Flow in Arteries*, London: Edward Arnold, 1960.

[6] R. Burattini, P. Borgdorff, D. R. Gross, B. Baiocco, and N. Westerhof, "Systemic autoregulation counteracts the carotid baroreflex," IEEE Trans. Biomed. Eng. 38: 47-55, 1971.

[7] S. J. Shin, W. N. Tapp, S. S. Reisman, and B. H. Hatelson, "Assessment of autonomic regulation of heart rate variability by the method of complex demodulation," IEEE Trans. Biomed. Eng. 36: 274-283, 1989.